

A novel fluorescent “turn-on” chemosensor for nanomolar detection of Fe(III) from aqueous solution and its application in living cells imaging

Jitendra Nandre^a, Samadhan Patil^a, Vijay Patil^a, Fabio Yu^b, Lingxin Chen^{*b}, Suban K Sahoo^c, Timothy Prior^d, Carl Redshaw^d, Pramod Mahulikar^{*a}, Umesh Patil^{*a}

^a School of Chemical Sciences, North Maharashtra University, P. B. No. 80, Jalgaon - 425 001, (MS), India. E-mail: mahulikarpp@rediffmail.com (PPM), udpatil.nmu@gmail.com (UDP).

^b Key Laboratory of Coastal Zone Environmental Processes and Ecological Remediation, Yantai Institute of Coastal Zone Research, Chinese Academy of Sciences, Yantai 264003, China. E-mail : lxchen@yic.ac.cn (LC).

^c Department of Applied Chemistry, S.V. National Institute Technology, Surat-395007, Gujrat, India. E-mail : suban_sahoo@rediffmail.com (SKS).

^d Department of Chemistry, University of Hull, Cottingham Road, Hull, HU6 7RX (UK).

Abstract

An electronically active and spectral sensitive fluorescent “turn-on” chemosensor (**BTP-1**) based on the benzo-thiazolo-pyrimidine unit was designed and synthesized for the highly selective and sensitive detection of Fe³⁺ from aqueous medium. With Fe³⁺, the sensor **BTP-1** showed a remarkable fluorescence enhancement at 554 nm ($\lambda_{ex} = 314$ nm) due to the inhibition of photo-induced electron transfer. The sensor formed a host-guest complex in 1:1 stoichiometry with the detection limit down to 0.74 nM. Further, the sensor was successfully utilized for the qualitative and quantitative intracellular detection of Fe³⁺ in two liver cell lines *i.e.*, HepG2 cells (human hepatocellular liver carcinoma cell line) and HL-7701 cells (human normal liver cell line) by confocal imaging technique.

Keywords: Fluorescent ‘turn-on’ sensor; benzo-thiazolo-pyrimidine; Fe³⁺; ICT; PET; live cells imaging.

1. Introduction

The development of highly selective and sensitive chemosensors for bioactive metal ions has gained enormous importance (Au-Yeung et al., 2013; Callan et al., 2005; Chen et al., 2012; Dutta and Das, 2012; Formica et al., 2012; Kim et al., 2012; Sahoo et al., 2012), as metal ions are well known to be involved in a variety of fundamental biological processes; which are essential for maintaining the life of organisms and remain sustainable in environmental conditions. As an important physiologically relevant metal ion, Fe^{3+} exhibits an obligatory role in many biochemical processes at the cellular level. Numerous enzymes use Fe^{3+} as a catalyst for electron transfer, oxygen metabolism, and RNA and DNA synthesis (Cairo and Pietrangelo, 2000; Crabtree, 1994). However, both its deficiency (hypoferremia) and excess (hyperferremia) can induce a variety of diseases. As a result of these concerns, intense research efforts have been focused on the development of highly sensitive and selective receptors for the qualitative and quantitative detection of Fe^{3+} . However, because of the paramagnetic nature of the Fe^{3+} ion, recognition of Fe^{3+} by fluorescence response is mostly signaled by a fluorescence quenching mechanism (Fan et al., 2006; Li et al., 2009; Lohani et al., 2009). Also, the design of a “turn-on” fluorescent chemosensor for the Fe^{3+} ion remains a challenging task for researchers working in the field of chemosensing due to the need to overcome the usual fluorescence quenching nature of Fe^{3+} . The lack of suitable “turn-on” fluorescent iron indicators is even more obvious when judged in terms of applications in bioimaging, although significant progress has been made on fluorescent molecular sensors for intracellular imaging of biologically important metal ions.

It is worth noting that many reported fluorescent “turn-on” chemosensors for the Fe^{3+} ion utilize the rhodamine moiety due to its advantageous photophysical properties (Sahoo et al., 2012). However, some rhodamine dyes are harmful if swallowed by humans or animals, and cause irritation of the skin, eyes and respiratory tract (Jain et al., 2007; Rochat et al., 1978). In

addition, among the various sensing methods, sensors based on a naked-eye response have many advantages because of their ability to provide a simple, sensitive, selective, precise and economical method for the detection of the target analyte without the use of sophisticated instrumentation. On the basis of previously reported data of Fe³⁺ chemosensors, herein, we focused on the development of a simple “turn-on” fluorescent chemosensor for Fe³⁺ ions from purely aqueous medium. To achieve this goal, we have designed and synthesized a novel benzo-thiazolo-pyrimidine based fluorescent sensor (**BTP-1**) for the selective recognition of Fe³⁺. The present sensor **BTP-1** is nontoxic and successfully used to study its *in vitro* glycosidase inhibitory activity (Patil et al., 2012).

2. Material and methods

2.1. Materials and Instrumentations

All the starting reagents and metal perchlorates were purchased either from S. D. Fine chemicals or Sigma Aldrich depending on their availability. All the reagents were used as received. All the solvents were of spectroscopic grade and were used without further treatment. The purity of the compounds and the progress of reactions were determined and monitored by means of analytical thin layer chromatography (TLC). Pre-coated silica gel 60 F₂₅₄ (Merck) on alumina plates (7x3 cm) were used and visualized by using either an iodine chamber or a short UV-Visible lamp. Melting points were recorded on the Celsius scale by open capillary method and are uncorrected. IR spectra were recorded on a Perkin-Elmer Spectrum One FT-IR spectrometer as potassium bromide pellets and nujol mulls, unless otherwise mentioned. IR bands are expressed in frequency (cm⁻¹). NMR spectra were recorded in CDCl₃ on a Varian (Mercury Vx) SWBB Multinuclear probe spectrometer, operating at 300 MHz and 75 MHz for ¹H NMR and ¹³C NMR, respectively and shifts are given in ppm downfield from TMS as an

internal standard. UV-Vis spectra were recorded on a U-3900 spectrophotometer (Perkin Elmer Co., USA) with a quartz cuvette (path length=1 cm). Fluorescence spectra were recorded on a Fluoromax-4 spectrofluorometer (HORIBA Jobin Yvon Co., France).

2.2. Spectroscopic Study

The receptor **BTP-1** was not soluble in water and therefore the stock solutions of **BTP-1** (1.0×10^{-3} M) was prepared in CH_3CN . All cations (1.0×10^{-2} M) solutions were prepared in water. These solutions were used for all spectroscopic studies after appropriate dilution. For the spectroscopic (UV-Vis and fluorescence) titrations, the required amount of the diluted receptor **BTP-1** (2 mL, 2×10^{-5} M, in CH_3CN) was taken directly into the cuvette and the spectra were recorded after each successive addition of cations (0-180 μL , 1×10^{-3} M, in H_2O) by using a micropipette.

2.3. Computational methods

All theoretical calculations were carried out using the Gaussian 09W computer program and the Gaussview 5.0.9 graphical interface (Frisch et al., 2009). Optimization of **BTP-1** and its complex with Fe^{3+} was carried out without symmetry constraints by applying the B3LYP/6-31G (d,p) method in the gas phase followed by the harmonic vibrational frequency which was calculated using the same methods to ascertain the presence of a local minimum. The basis set LANL2DZ was used for Fe^{3+} atom.

2.4. Living cells imaging

The solution of **BTP-1** (DMSO, 1.0 mM) was prepared and maintained in a refrigerator at 4°C . FeCl_3 is as the iron-supplemented source. The confocal fluorescent images were acquired on an Olympus laser-scanning microscope with an objective lens (x40). Excitation of the probe was carried out using a Spectra Physics InSightDeepSee ultrafast laser at 700 nm and emission

was collected between 500 and 600 nm. Prior to imaging, the medium was removed. Cell imaging was carried out after washing cells with RPMI-1640 for three times.

Cell Culture: HepG2 cells (Human hepatocellular liver carcinoma cell line) and HL-7701 cells (human normal liver cell line) were purchased from the Committee on type Culture Collection of Chinese Academy of Sciences. Cells were seeded at a density of 1×10^6 cells/mL for confocal imaging in RPMI 1640 medium supplemented with 20 % fetal bovine serum (FBS), NaHCO_3 (2 g/L), and 1 % antibiotics (penicillin /streptomycin, 100 U/ml). Cultures were maintained at 37 °C under a humidified atmosphere containing 5 % CO_2 . The cells were sub-cultured by scraping and seeding on 15 mm petri-dishes according to the instructions from the manufacturer.

2.5. Synthesis of **BTP-1**

Synthesis of **BTP-1** was achieved by using a mild base through ring transformation of suitably functionalized 4-(methylthio)-2-oxo-6-naphthyl-2*H*-pyran-3-carbonitriles (**2**) with 2-amino-benzothiazole in DMF using DBU as the base (Scheme 1) (Patil et al., 2012). The precursors, 4-(methylthio)-2-oxo-6-naphthyl-2*H*-pyran-3-carbonitriles (**2**) was prepared by stirring an equimolar mixture of ethyl 2-cyano-3,3-bis(methylthio)acrylate (**1**), substituted acetophenone and KOH in DMF (Tominaga et al., 1984).

Synthesis of ethyl 2-cyano-3,3-bis(methylthio)acrylate (1): In a 250 ml beaker, a mixture of water (10 mL) and DMF (30 mL) and KOH (9.87 g, 176 mmol) were cooled to 0 °C. Ethyl 2-cyanoacetate (10 g, 88 mmol) was added dropwise to this cold solution over 30 min., and stirred for 10-15 min. Then carbon disulfide (6.70 g, 88 mmol) was added dropwise for 20 min. at 0 to -5 °C. The mixture was stirred for 60 min. at room temperature, and then reaction mixture was again cooled to 0 °C and dimethyl sulphate (22.20 g, 176 mmol) was added dropwise over 30 min. The reaction mixture was allowed to stand at room temperature for 12 h and then it was

poured into crushed ice cold water (400 mL) and kept at room temperature with vigorous stirring for 10-15 min. The obtained yellowish solid was filtered, washed with cold water and dried. The crude product was recrystallized from methanol.

Synthesis of 6-naphthyl-3-cyano-4-methylthio-2H-pyran-2-ones (2): In a 100 ml round bottom flask, a mixture of 2-acetyl naphthalene (1.7 g, 0.01 mol) and ethyl 2-cyano-3,3-bis(methylthio)acrylate (2.17 g, 0.01 mol, **1**), powdered KOH (1.12 g, 0.02 mol) and 50 mL of dry DMF was stirred at room temperature for 5-6 h. Progress of the reaction was monitored by TLC (ethyl acetate : hexane, 3:7). After completion of the reaction, the reaction mixture was poured onto crushed ice (500 mL of ice-water) with vigorous stirring and then it was stirred at room temperature for 4-5 h. The yellow precipitate formed was filtered, washed with cold water and dried. The crude product was recrystallized from methanol.

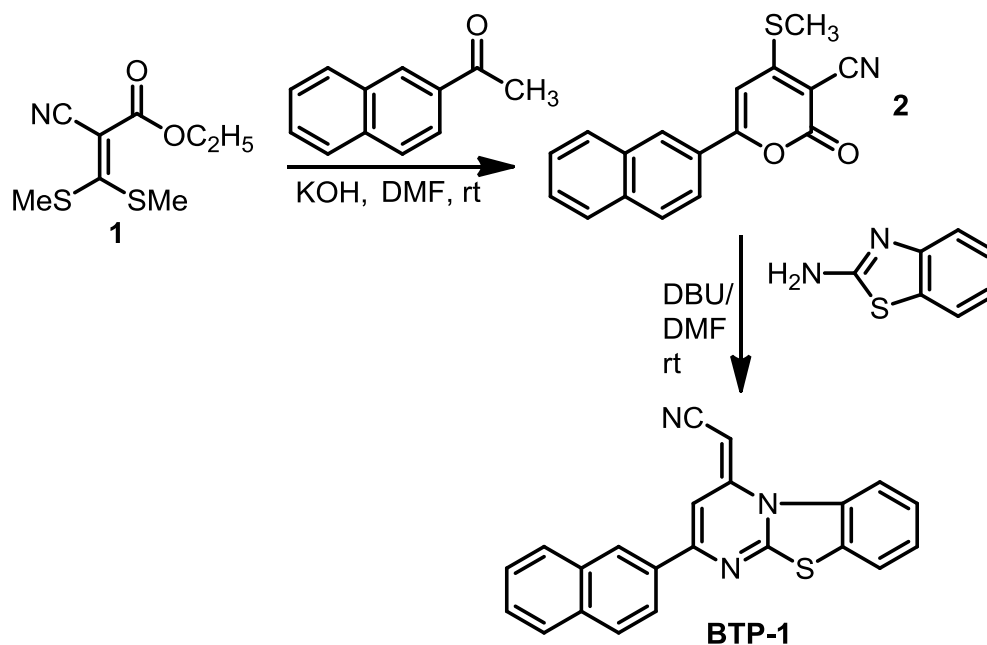
*Synthesis of **BTP-I**:* A mixture of 2-aminobenzothiazole (1 mmol) and DBU (2 mmol) and DMF (15 mL) was stirred under nitrogen flux for 10-15 min. at room temperature. Then 4-(methylthio)-2-oxo-6-naphthalen-2H-pyran-3-carbonitrile (**2**, 1 mmol) was added under nitrogen flux with constant stirring. The progress of the reaction was monitored by TLC (ethyl acetate: hexane, 2:8). After completion of the reaction (about 4-12 h), the reaction mixture was poured onto crushed ice with vigorous stirring about 30 min. The reaction mixture was allowed to stand at room temperature for about 20 min. to settle down the solid, which was the isolated by filtration. The obtained crude product was dissolved in hot MeOH (70 mL) and filtered. The collected insoluble solid was again dissolved in to hot chloroform (40 mL), filtered rapidly (impurity remains insoluble in hot chloroform while product is soluble) and cooled. Chloroform was removed to afford the pure product. **Mol. Formula:** C₂₂H₁₃N₃S; **Mol. Weight:** 351.42 g; **Physical Nature:** Yellow solid; **IR (cm⁻¹) [KBr]:** 2923, 2178, 1599, 1526, 1267; **Mass [ESI, 70 Ev] m/z (%):** 353 (30), 352 (100), 291 (45), 153 (25); **¹H NMR (300 MHz, CDCl₃, δ ppm):**

5.15 (s, 1H, CH=C), 7.43 (s, 1H, PhH), 7.45-7.55 (m, 4H, PhH), 7.69-7.71 (dd, $J=1.3$ Hz, $J=7.5$ Hz, 1H, PhH), 7.86-8.06 (m, 5H, PhH), 8.58 (s, 1H, PhH); ^{13}C NMR (75 MHz, CDCl_3 , δ ppm): 64.2, 104.4, 115.7, 119.5, 122.9, 123.3, 125.1, 126.4, 126.5, 127.0, 127.2, 127.6, 128.2, 128.4, 128.9, 132.2, 133.1, 134.2, 135.5, 150.1, 151.9, 160.4; **HRMS (ESI): m/z** : Calculated for $\text{C}_{22}\text{H}_{14}\text{N}_3\text{S}_1$: $[\text{M}+\text{H}]^+$ 352.0920, Found: 352.090

3. Results and discussion

3.1. Synthesis of **BTP-1**

Synthesis of **BTP-1** was achieved by using a mild base DBU through ring transformation of a suitably functionalized 4-(methylthio)-2-oxo-6-naphthyl-2H-pyran-3-carbonitriles (**2**) with 2-aminobenzothiazole in DMF (Scheme 1). The structure of **BTP-1** was characterized by IR, ^1H -NMR and ^{13}C -NMR spectroscopy and HRMS (Figure S1, S2, S3, S4 and S5[†]). Finally, suitable crystal of **BTP-1** for a single crystal X-ray diffraction[‡] study was obtained from chloroform, and the molecular structure was shown in Fig. S6[†].



Scheme 1. Synthesis of **BTP-1**.

3.2. Naked-eye selectivity study of **BTP-1**

The recognition properties of **BTP-1** (2 mL, 2×10^{-5} M, in CH_3CN) toward different metal ions (20 μL , 1×10^{-2} M, in H_2O) were studied experimentally by naked-eye, UV-Visible, and fluorescence methods. In the naked-eye experiments (Figure S7[†]), no obvious visual color changes of **BTP-1** were observed in the presence of the tested metal ions. However, under UV light, sensor **BTP-1** showed a selective “turn-on” fluorescence upon addition of Fe^{3+} over other tested metal ions (Ag^+ , Ca^{2+} , Cd^{2+} , Co^{2+} , Cs^+ , Cu^{2+} , Fe^{2+} , Hg^{2+} , K^+ , Li^+ , Mg^{2+} , Mn^{2+} , Ni^{2+} , Pd^{2+} and Zn^{2+}). The observed fluorescence intensity reveals that the receptor **BTP-1** shows higher recognition ability for Fe^{3+} . Interestingly, this fluorescence “turn-on” response becomes reversibly “turn-off” after the addition of an aq. solution of EDTA. Encouraged by the Fe^{3+} selective and reversible response shown by **BTP-1**, the quantitative and qualitative metal ions sensing behavior of **BTP-1** was determined further by spectrophotometric methods.

3.3. UV-Visible absorption study of **BTP-1**

Sensor **BTP-1** exhibited two absorption bands, one at 313 nm and a weak narrow band at 271 nm. On addition of 5 equivalents of Fe^{3+} ions (20 μL , 1×10^{-2} M, in H_2O) to the solution of **BTP-1** (2 mL, 2×10^{-5} M, in CH_3CN), significant spectral changes were observed (Fig. 1 & S8[†]). A hypochromic shift was observed at 271 nm while the band at 313 nm was disappeared completely and a new broad band appeared between 350 nm to 425 nm. The red shifted band was observed presumably due to the delocalization of electrons from the nitrile nitrogen on formation of complex species with Fe^{3+} (Fig. S9[†]), which was supported by comparing the variations in the bond lengths of the DFT optimized structure of **BTP-1** and Fe^{3+} .**BTP-1** complex (Fig. S10[†]). Moreover, the red-shift can also be explained due to the intramolecular charge transfer (ICT) process and the lowering of the band gap between HOMO and LUMO on complexation with Fe^{3+} (Fig. S11[†]). **This effective ICT induced by the electron push-pull system**

(Lin et al., 2008). As in $-\text{CN}$ group, the presented nitrogen is having sp hybridization so less willing to bind with metal cations as compare to sp^2 nitrogen and sulfur. Importantly, no distinguishable spectral changes were observed in the presence of other tested metal ions.

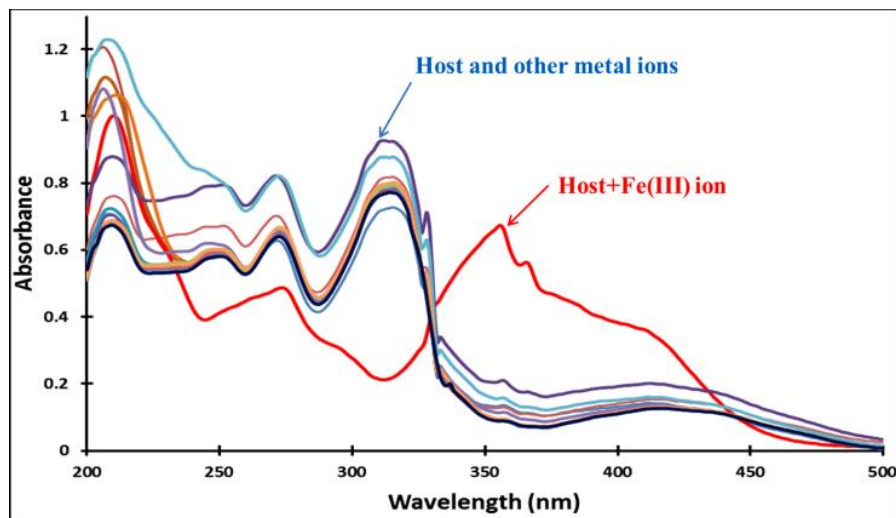


Fig. 1. Changes in the absorbance of **BTP-1** (2 mL, 2×10^{-5} M, in CH_3CN) in absence and presence of 5 equivalents of different metal ions (20 μL , 1×10^{-2} M, in H_2O).

The absorption titration of **BTP-1** (2 mL, 2×10^{-5} M, in CH_3CN) was next performed with incremental addition of Fe^{3+} (Fig. 2). The spectral changes with the formation of an isosbestic point at 328 nm indicate the formation of a single complex species between sensor **BTP-1** and added Fe^{3+} . From the absorption titration of **BTP-1**, the limit of detection (LOD) and quantification (LOQ) of Fe^{3+} was calculated to be 0.10 μM and 0.32 μM , respectively based on the ICH Q2B recommendations by using the equations: $\text{LOD} = 3.3 \sigma / S$ and $\text{LOQ} = 10 \sigma / S$. Where, S and σ represents the slope and the standard deviation of the intercept of regression line of the calibration curve (Fig. S12†). This detection limit is acceptable within the US EPA limit (0.3 mg/L, equivalent to 5.4 μM) for the detection of Fe^{3+} in drinking water. Further, the Jobs'

plot (Fig. S13†) and LCMS (Fig. S14†) analysis was performed, which suggested that there was only one type of 1:1 binding interaction between the sensor **BTP-1** and Fe^{3+} .

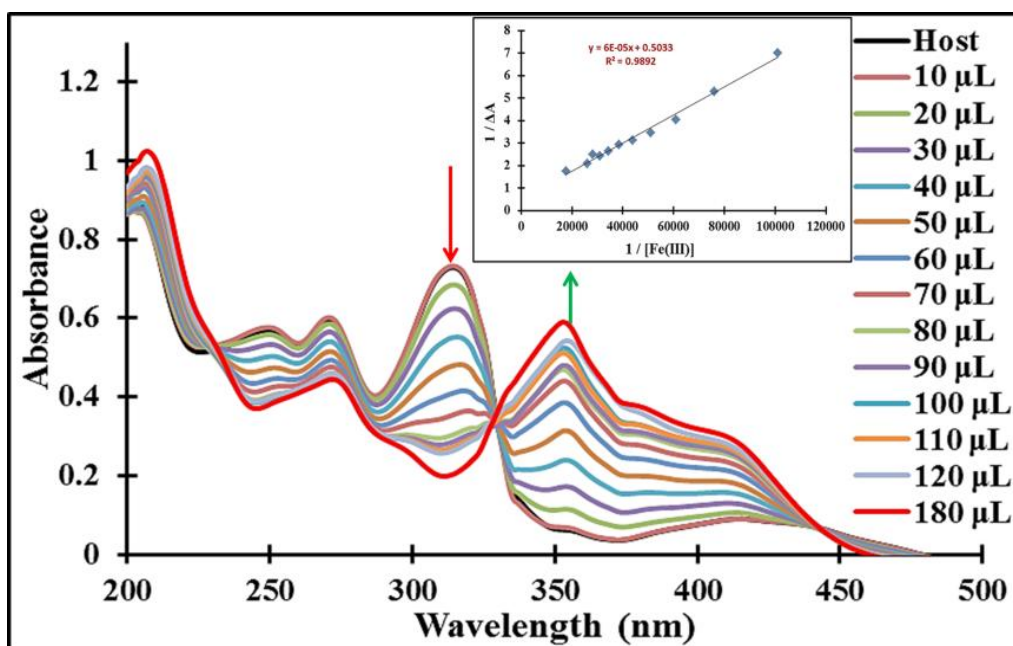


Fig. 2. Absorbance titration of **BTP-1** (2×10^{-5} M, in CH_3CN) upon the addition of incremental amount of Fe^{3+} (0-180 μL , 1×10^{-3} M, in H_2O). Inset showing the Benesi-Hildebrand plot.

3.4. Emission spectroscopic study of **BTP-1**

The cation binding behavior of **BTP-1** was also investigated by fluorescence spectroscopy. We observed a remarkable fluorescence enhancement of **BTP-1** (2 mL, 2×10^{-5} M, in CH_3CN) at 554 nm ($\lambda_{\text{ex}} = 314$ nm) upon addition of Fe^{3+} (20 μL , 1×10^{-2} M, in H_2O) due to the inhibition of photo-induced electron transfer (PET) from electron-donating nitrogen to electron-receptor naphthalene ring (Li et al., 2011), while no significant changes were observed in the presence of other tested metal ions (Fig. 3 & S15†). The fluorescence titration experiment of **BTP-1** with Fe^{3+} showed a ≈ 10 -fold fluorescence enhancement at 554 nm (Fig. 4). The binding constant (K) of **BTP-1** with Fe^{3+} was determined by a Benesi-Hildebrand plot analysis of both absorption (Fig. 2, inset) and fluorescence titrations data (Fig. S16†); additional data was

obtained via a Scatchard plot from fluorescence titration data (Fig. S17†). The cation binding affinity of **BTP-1** was found to be $\approx 4 \times 10^4 \text{ M}^{-1}$ for Fe^{3+} .

Based on the fluorescence titration, the LOD and LOQ of **BTP-1** for Fe^{3+} was found to be 0.74 nM and 2.23 nM, respectively, and these values are quite better than the reported sensors (Table S1†). Further, the effect of coexisting biologically relevant metal ions on the detection of Fe^{3+} by **BTP-1** was investigated. In a CH_3CN solution of **BTP-1** (2 mL, $2 \times 10^{-5} \text{ M}$, in CH_3CN), the addition of 2 equivalents of Fe^{3+} (8 μL , $1 \times 10^{-2} \text{ M}$, in water) in the presence of 2 equivalents of other tested metal ions (8 μL , $1 \times 10^{-2} \text{ M}$, in water) caused a dramatic enhancement in the fluorescence intensity of **BTP-1** with only very slight or no interference effects (Fig. S18†). Therefore, we conclude that **BTP-1** is a reliable, highly selective and sensitive “turn-on” fluorescent sensor for Fe^{3+} .

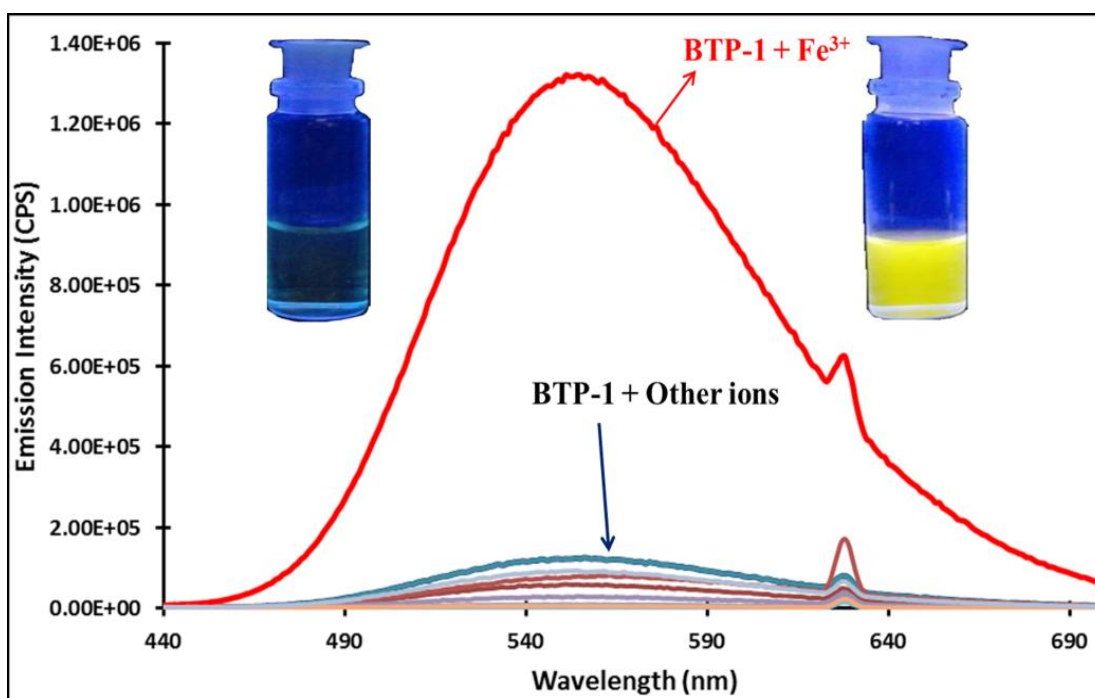


Fig. 3. Fluorescence emission change of sensor **BTP-1** (2 mL, $2 \times 10^{-5} \text{ M}$, CH_3CN) upon the addition of a particular metal ions (20 μL , $1 \times 10^{-2} \text{ M}$, in H_2O), $\lambda_{\text{ex}} = 314 \text{ nm}$.

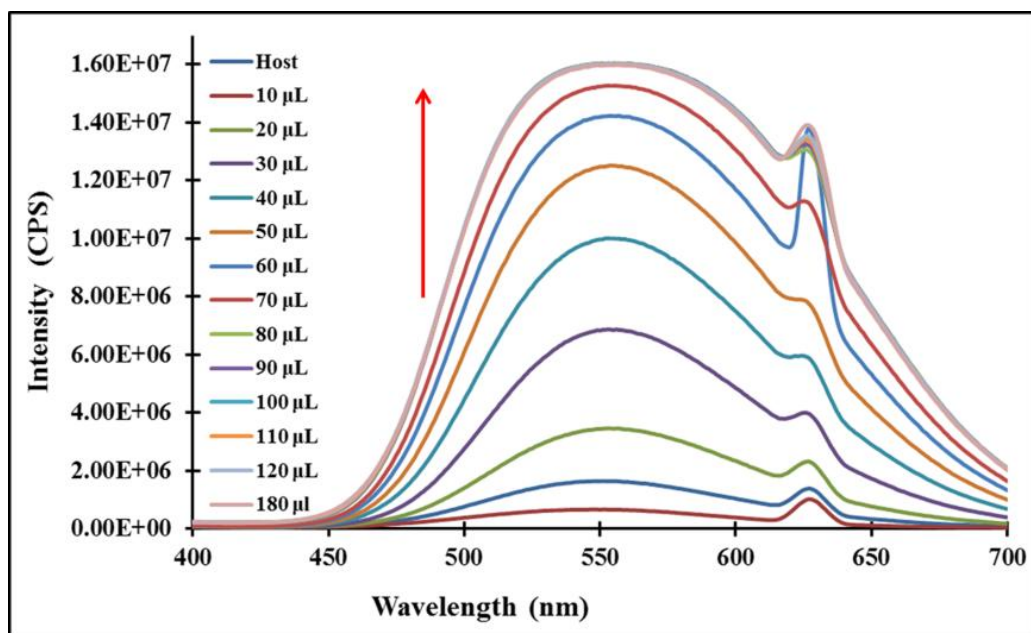


Fig. 4. Changes in fluorescence emission intensity of **BTP-1** (2 mL, 2×10^{-5} M, in CH_3CN) upon the addition of incremental amount of Fe^{3+} (0-180 μL , 1×10^{-3} M, in H_2O).

3.5. Live cells imaging study of **BTP-1**

The fluorescent behavior of **BTP-1** was applied for the intracellular detection and monitoring of Fe^{3+} in two liver cell lines *i.e.*, HepG2 cells (human hepatocellular liver carcinoma cell line) and HL-7701 cells (human normal liver cell line). The HepG2 cells in Fig. 4b and 4d were incubated with 0.01 μM and 100 μM Fe^{3+} for 30 min in RPMI 1640 medium at 37°C , and then washed with RPMI 1640 to remove excess Fe^{3+} . After being incubated with **BTP-1** (10 μM) in RPMI 1640 for 10 min, the cells were imaged by a confocal fluorescence microscope. As shown in Fig. 5, there is a significant intracellular fluorescence increase revealed in Fig. 5b and 5d compared with the control cells in Fig. 5a, which indicates the ability of **BTP-1** to detect intracellular Fe^{3+} . Further, to confirm that the increase in the fluorescence depended on the Fe^{3+} changes, the iron-supplemented cells in Fig. 5b and 5d were treated with 50 μM of iron chelator desferoxamine (DFO) for 40 min to remove the intracellular levels of Fe^{3+} . As expected, the DFO chelation shrunk the cellular fluorescence (Fig. 5c and 5e), indicating that the observed

fluorescence enhancements (Fig. 5b and 5d) were due to the changing levels in the Fe^{3+} -supplemented cells.

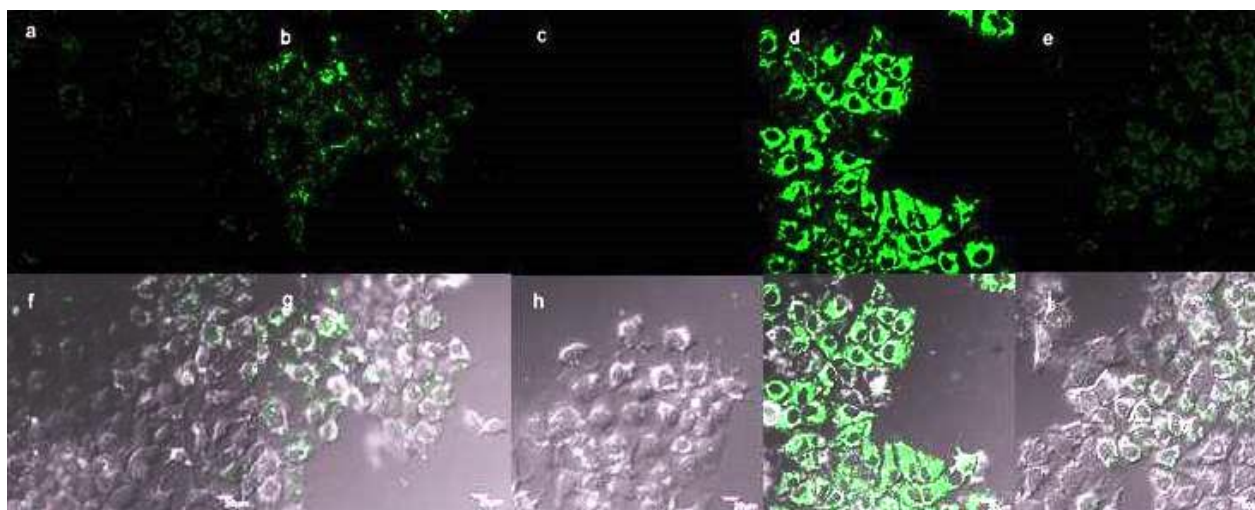


Fig. 5. Fluorescence confocal microscopic images of living HepG2 cells incubated with Fe^{3+} . (a) Cells loaded with 10 μM **BTP-1** for 10 min as control. (b) and (d), Cells loaded with 0.1 μM and 100 μM Fe^{3+} for 30 min, then 10 μM **BTP-1** for 10 min. (c) and (e), Cells were treated as (b), then loaded with 50 μM of iron chelator desferoxamine (DFO) for 40 min. (f)-(g) Overlays of bright field images and fluorescence channels in (a)-(e). Scale bar is 20 μm .

After establishing that the sensor **BTP-1** can detect Fe^{3+} within living HepG2 cells, we turned our attention to quantify the cellular Fe^{3+} level changes in HL-7701 cells. The relative fluorescence intensity of the confocal microscopy images in Fig. 6 were evaluated by Image-Pro Plus software (Fig. 6i). HL-7701 cells were treated with different concentrations of Fe^{3+} , and then loaded with 10 μM **BTP-1** for 10 min following which the cells were washed three times with RPMI-1640 before imaging (Fig. 6). Cells in Fig. 6b were as control, which showed almost no fluorescence after treated with 50 μM of DFO (Fig. 6a). Our sensor might also detect Fe^{3+} at basal, endogenous levels within cells. Therefore, we selected the cell-body regions in the visual field (Fig. 6a-h) as the region of interest to determine the average fluorescence intensity. The

confocal fluorescence images became gradually brighter as the concentration of Fe^{3+} increased from 0.01 μM to 100 μM Fe^{3+} (Fig. 6c-g), and then the fluorescence intensity becomes saturated after 100 μM Fe^{3+} (Fig. 6h). Taken together, these quantitative assays established that the sensor **BTP-1** can be used for the fluorescence detection of Fe^{3+} level changes within living cells. The results also suggest that our sensor has good membrane permeability.

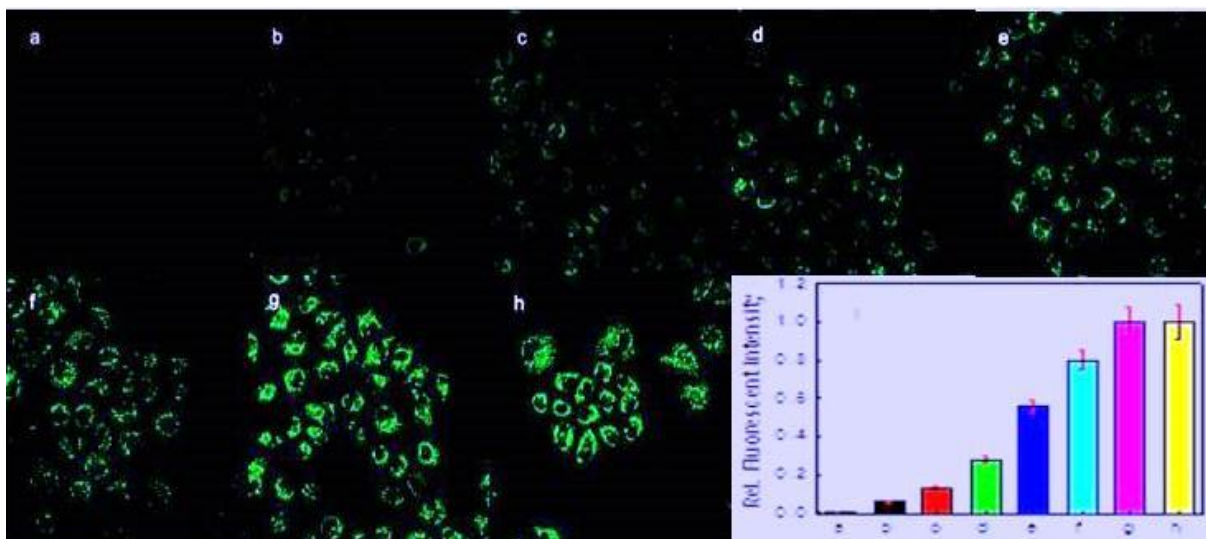


Fig. 6. Fluorescence confocal microscopic images of living HL-7701 cells incubated with various concentrations of Fe^{3+} . (a) Cells loaded with 50 μM of iron chelator desferoxamine (DFO) for 40 min. (b) Cells loaded with 10 μM **BTP-1** for 10 min as control. (c) - (h) Cells incubated with 0.01, 0.1, 1, 10, 100 and 1000 μM Fe^{3+} , respectively. (i) Quantification of mean fluorescence intensity in Fig. S20a-S20h correspondingly. Scale bar is 20 μm .

4. Conclusions

In conclusion, we have developed a simple benzo-thiazolo-pyrimidine based Fe^{3+} -selective fluorescent ‘turn-on’ sensor **BTP-1**. Sensor **BTP-1** showed an excellent selectivity for Fe^{3+} over other interfering metal ions with the detection limit down to nanomolar concentration. Also, the sensor works well in the pH range of 6-8. Confocal microscopy images indicate that

BTP-1 can be used for detecting changes in Fe^{3+} levels within living cells. To the best of our knowledge, this is the first example of a chromo-fluorogenic sensor based on benzo-thiazolo-pyrimidine that allows the selective detection of the Fe^{3+} ion by a fluorescence “turn-on” mode in live cells. Based on the bioactive molecules like benzo-thiazolo-pyrimidine, sensor **BTP-1** with its low cost and easy preparation, its excellent selectivity and low detection limit, suggests this approach could potentially lead to many more sensors being designed using the benzo-thiazolo-pyrimidine as a core skeleton.

Acknowledgments:

The author Dr. U. D. Patil is grateful for the financial support from the Department of Science & Technology, New Delhi, India (Reg. No. CS-088/2013). We thank the EPSRC National Crystallographic Service (Southampton, UK) for data.

Appendix A. Supporting information

Supplementary data associated with this article can be found in the online version at <http://dx.doi.org/10.xxxx/j.bios.2014.10.070>. †Synthesis details, experimental details, sensing supporting results, DFT images, and additional spectroscopic data. ‡CCDC 985967 contains the supplementary X-ray data for this paper. These data can be obtained free of charge via (please use the link below) by e-mailing data_request@ccdc.cam.ac.uk, or by contacting: The Cambridge Crystallographic Data Centre, 12 Union Road, Cambridge.CB2 1EZ, UK. Fax: +44(0)1223-336033. www.ccdc.cam.ac.uk/data_request/cif. This material is available free of charge via the Internet at.

References

- Au-Yeung, H.Y., Chan, J., Chantarojsiri, T., Chang, C.J., 2013. *Journal of American Chemical Society* 135, 15165-15173.
- Cairo, G., Pietrangelo, A., 2000. *Biochemical Journal* 352, 241-250.
- Callan, J.F., Silva, A.P., Magri, D.C., 2005. *Tetrahedron* 61, 8551-8588.
- Chen, X., Pradhan, T., Wang, F., Kim, J.S., Yoon, J., 2012. *Chemical Reviews* 112, 1910-1956.
- Crabtree, H.H., 1994. *Science* 266, 1591-1592.
- Dutta, M., Das, D., 2012. *Trends in Analytical Chemistry* 32, 113-132.
- Fan, L.F., Wayne, J., Jones, E., 2006. *Journal of American Chemical Society* 128, 6784-6785.
- Formica, M., Fusi, V., Giorgi, L., Micheloni, M., 2012. *Coordination Chemistry Reviews* 256, 170-192.
- Frisch, M.J. et. al., 2009. *Gaussian 09, G09W®*, Gaussian Inc., Wallingford, USA.
- Jain, R., Mathur, M., Sikarwar, S., Mittal, A., 2007. *Journal of Environmental Management* 85, 956-964.
- Kim, H.N., Ren, W.X., Kim, J.S., Yoon, J., 2012. *Chemical Society Reviews* 41, 3210-3244.
- Li, N., Xu, Q., Xia, X., Wang, L., Lu, J., Men, X., 2009. *Materials, Chemistry and Physics* 114, 339-343.
- Li, Z.-X., Zhang, L.-F., Zhao, W.-Y., Li, X.-Y., Guo, Y.-K., Yu, M.-M., Liu, J.-X., 2011. *Inorganic Chemistry Communications* 14, 1656-1658.
- Lin, W., Yuan, L., Cao, X., 2008. *Tetrahedron Letters* 49, 6585-6588.
- Lohani, C.R., Kim, J.-M., Lee, K.-H., 2009. *Bioorganic Medicinal Chemistry Letters* 19, 6069-6073.
- Patil, V.S., Nandre, K.P., Ghosh, S., Rao, V.J., Chopade, B.A., Bhosale, S.V., Bhosale, S.V., 2012. *Bioorganic Medicinal Chemistry Letters* 22, 7011-7014.

Rochat, J., Demenge, P., Rerat, J.C., 1978. *Toxicological European Research* 1, 23-26.

Sahoo, S.K., Sharma, D., Bera, R.K., Crisponic, G., Callan, J.F., 2012. *Chemical Society Reviews* 41, 7195-7227.

Tominaga, Y., Ushirogochi, A., Matsuda, Y., Kobayashi, G., 1984. *Chemical and Pharmaceutical Bulletin* 32, 3384-3395.